

## A CLOSED LOOP CONTROL STRATEGY FOR A FREQUENCY-ONLY CONVERTER WITH HIGH EFFICIENCY

Aziza Benaboud  
 Industrial Electronics Laboratory (LEI)  
 Ecole Polytechnique Fédérale de Lausanne, Switzerland  
 email: aziza.benaboud@epfl.ch

Alfred Rufer  
 Industrial Electronics Laboratory (LEI)  
 Ecole Polytechnique Fédérale de Lausanne, Switzerland  
 email: alfred.rufer@epfl.ch

### ABSTRACT

Many electric power generators use gas turbines as power sources, coupled through a mechanical gearbox in order to adapt their synchronous speed to the optimal rotation speed of the turbine. This paper proposes to replace the mechanical gearbox with a flexible electronic solution which would offer a higher efficiency. A new control strategy is proposed for the three level Neutral Point Clamped converter, which is characterized by its high efficiency due to the use of square-wave modulation. The main advantage of this modulation is the quasi absence of switching losses. In this modulation, only the frequency can be adapted between the input and the output voltages, but their magnitudes are not freely controllable. The active and reactive powers produced can be controlled by the generator's excitation, as well as both the angle shift between the generator's and rectifiers's voltages and between the inverter's and network's voltages. The simulation and a partial experimental results for different operating points highlight the capabilities of the proposed control strategy.

### KEY WORDS

NPC, three level converter, Square Wave Modulation, high efficiency, angle shift control, closed loop control.

### 1. Introduction

Due to its significant advantages in high-power, medium and high voltage applications, the three level Neutral Point Clamped (NPC) converter has received special attention during the last two decades [1] [2]. With the NPC topology, three level converters allow the output voltage to spread on three levels and thus increase it above the voltage limits of classical semiconductors and also reduce its harmonic distortion. However, this type of converter is not common because it produces very high switching losses due to the high frequency of the PWM technique, normally used for its control. This paper describes a new control strategy for a special frequency converter. By using a Square Wave Modulation (SWM) at both the input and the output sides, the ratio between input and output voltage is kept constant [3][4]. Figure 1 illustrates the schematic diagram of such a frequency converter, used as an interface between a fast running synchronous generator and the grid. In this application, the converter can be designated as a “frequency

only converter”, due to the fixed ratio between the input and output voltage magnitudes. Voltage adaptation, which is used for the power flow control through the network, can be achieved by changing the generator's excitation.

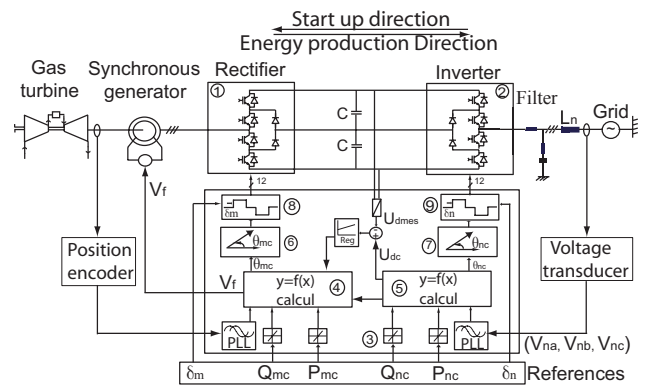


Figure 1. Schematic diagram of the final application using three level converter.

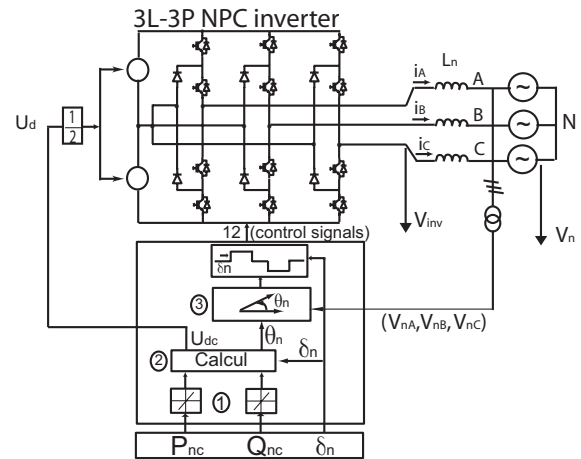


Figure 2. Schematic diagram of the proposed control strategy for 3L3P NPC inverter.

Both input and output converters are controlled in the same manner. Therefore, only the line side control of the output converter is described in this paper. To simplify, the generator and its rectifier will be replaced with an adjustable DC voltage source at the input of the inverter. Figure 2 presents the schematic diagram of the proposed control strategy for the three level three phases NPC inverter.

This paper is organized as follows: Section 2 presents the high power converter topologies using three level NPC converter in square wave modulation. Section 3 proposes a method to reduce the harmonics distortion of the inverter output voltage in SWM. Section 4 describes the control strategy and presents some limitations and control error incurred using an open loop circuit. Section 5 presents a closed loop control strategy including dynamic regime, and Section 6 shows some verification results. Finally, Section 7 concludes the paper.

## 2. Three-level neutral point clamped inverter for high power application

A three level Neutral Point Clamped inverter is widely used for medium voltage applications. It allows the output voltage to spread on three levels and thus to increase it above the voltage limits of classical semiconductors.

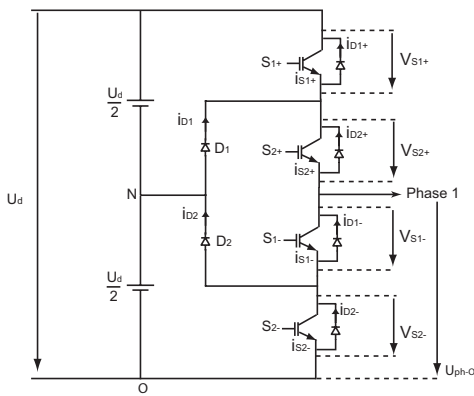


Figure 3. Phase circuit diagram of a three level NPC inverter.

Figure 3 shows the main circuit of the NPC inverter, where for clarity only one phase is shown. In this configuration, the DC side will be connected to the capacitor midpoint N (neutral point) via diodes to provide the third level in the output waveform.

For high power applications, for example: (73MVA (9.4kV, 5.23kA)), high voltage IGBTs are needed. To achieve the required output voltages of (9.4kV), which means DC-link voltages above 15 kV, the use of three level technology with the available 2.5 kV and 2 kA devices [5], is not sufficient, so an internal series connection is necessary (see Figure 4). In addition, to fulfill the demands of high power applications, it is necessary to use several leg modules in parallel (see Figure 5). This solution allows the output voltage and current to increase above the semiconductors limits, so that it can be used for high power applications. However, the series connection of power semiconductors can have negative side effects, such as power semiconductors voltage equilibrium. To ensure the voltage stabilization between the power semiconductors, an appropriate converter control method is needed.

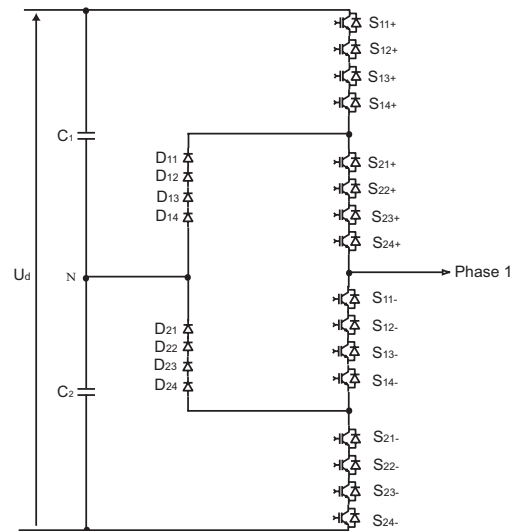


Figure 4. Phase circuit diagram of a three level NPC inverter, with internal series connections.

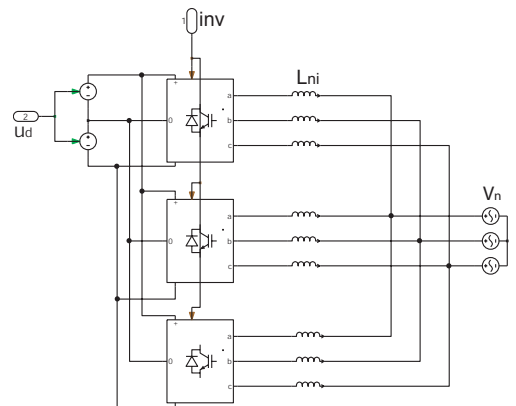


Figure 5. Three blocs of 3L-3P-NPC inverter operating in parallel.

In order to have an estimation of the converter efficiency, the model in Figure 5 has been simulated using the following characteristics:  $V_n = 9.4kV$  is the network voltage.  $I_n = 5.23kA$  is the line current.  $L_{ni} = 1.71mH$  is the line inductance.  $S_n = \frac{3}{2}V_n I_n = 73.8MVA$  is the apparent power.  $U_d = 15kV$  is the DC voltage at the input of the inverter. The semiconductors used in this model: are IGBT (5SNR20H2500) [5], and they are driven by using a square wave modulation.

Figure 6 plots our results: the active and reactive powers are represented, together with total losses calculated using the model in Figure 5. In comparison with a maximal power, the total losses in this converter represent only 0.21%, which means approximately 99.97% efficiency. It is important to notice that for a complete back to back frequency converter, the produced power is affected twice by this efficiency value, i.e. 99.5%. This high efficiency is achieved by the use of Square Wave Modulation which yields a quasi absence of switching losses.

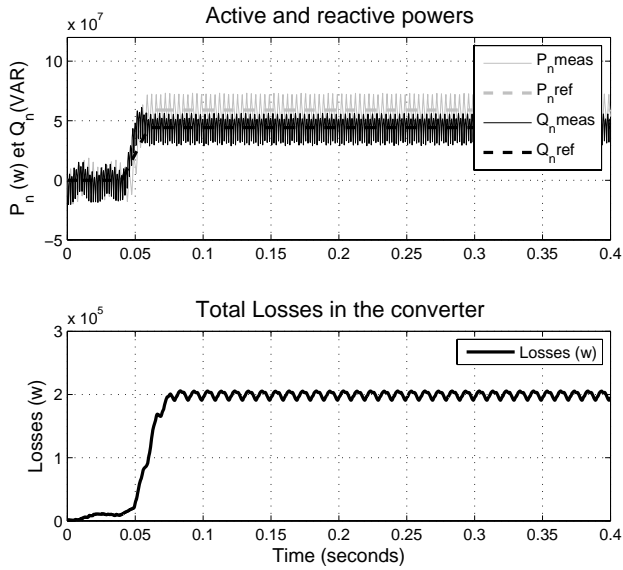


Figure 6. Active and reactive powers and converter losses.

### 3. Square wave modulation

As already mentioned in Figure 3, the DC side of the three level inverter will be connected to the midpoint N via diodes to provide the third level for the output waveform. Figure 7 shows an output-voltage's waveform of a three-level converter operated in square-wave mode.

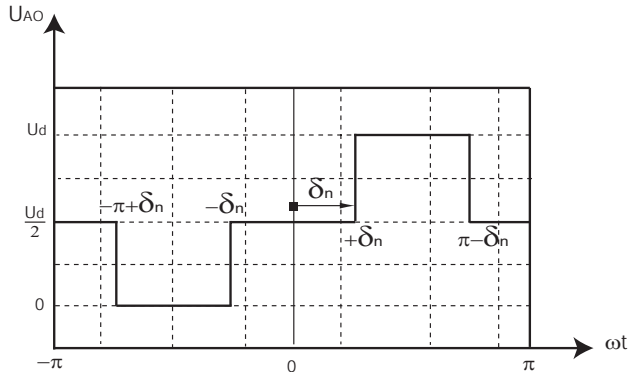


Figure 7. Output-voltage waveform  $U_{AO}$  of three-level converter operated in SWM.

In this figure,  $\delta_n$  represents a selected switching angle, which depends on the harmonics component according to (2) derived from (1) [6].

$$\nu \hat{U} = \frac{1}{\pi} \int_{-\pi}^{\pi} U_{AO} \sin \nu \omega t d\omega t \quad (1)$$

$$\nu \hat{U} = \frac{2}{\nu \pi} U_d \cos \nu \delta \quad (2)$$

Two important criteria must be taken into consideration when selecting the switching angle: fundamental volt-

age evolution and harmonic distortion (THD) of the output voltage. To illustrate this point, Figure 8 presents in function of the switching angle, the ratio between the fundamental wave  ${}^1\hat{U}$  and the DC voltage  $U_d$  given by (3). The THD of the output voltage according to (4) is also represented.

$$\frac{{}^1\hat{U}}{U_d} = \frac{2}{\pi} \cos \delta_n \quad (3)$$

$$THD = \frac{100}{\cos \delta_n} \sqrt{\sum_{\nu=5}^{\infty} \left( \frac{\cos(\nu \delta_n)}{\nu} \right)^2} \% \quad (4)$$

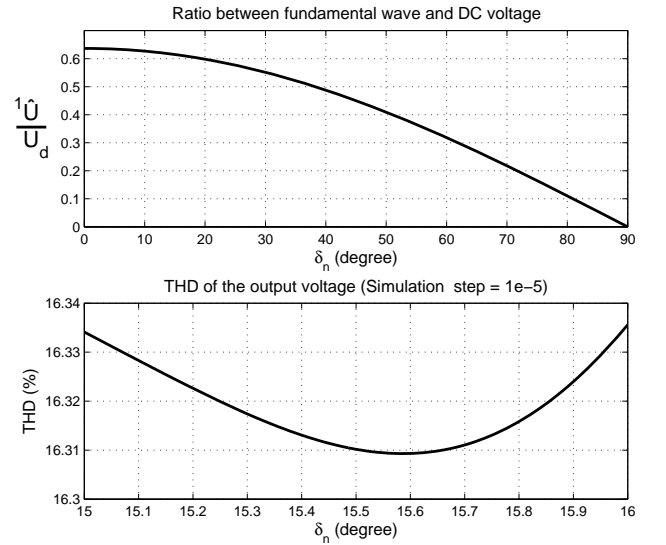


Figure 8. The fundamental and the THD of the output voltage as a function of the switching angle  $\delta_n$ .

The curve in Figure 8 shows that the ratio (3) hardly changes, as a function of  $\delta_n$ , in the range between  $0^\circ$  and  $20^\circ$ . In this range the output voltage's THD presents a minimum value, exactly when  $\delta_n = 15.58$ . The switching angle  $\delta_n$  can also be optimized to eliminate some harmonics. For example, the 5<sup>th</sup> harmonic disappears when  $\delta_n = 18^\circ$ .

By choosing the switching angle, the minimum of harmonics can be obtained ( $\delta_n = 15,58^\circ \Rightarrow THD = 16\%$ ). The traditional two level converter has more harmonic contents, which corresponds to ( $\delta_n = 0^\circ \Rightarrow THD = 31\%$ ). The advantage of this method with SWM is that the lower harmonics are reduced or eliminated without increasing the higher-order harmonics, contrary to what occurs in many PWM techniques. The disadvantage is that the fundamental output voltage is not freely controllable, it must be controlled by varying the DC link voltage. This point will be described in the next section.

## 4. Proposed control strategy

### 4.1 Description

As illustrated in Figure 2, the 3L-3P-NPC inverter is connected to the grid via inductances and fed by an adjustable DC voltage source  $U_d$ . Its control is based on an angular shift between the grid and the inverter output voltages, and on the DC voltage magnitude's adaptation [7].

$$\begin{cases} \theta_{nc} = \arctan \left( \frac{P_{nc}}{\frac{3}{2} \frac{V_n^2}{X_n} - Q_{nc}} \right) \\ U_{dc} = \frac{\pi}{2 \cos \delta_n} \sqrt{\left( V_n - \frac{2}{3} \frac{X_n}{V_n} Q_{nc} \right)^2 + \left( \frac{2}{3} \frac{X_n}{V_n} P_{nc} \right)^2} \end{cases} \quad (5)$$

The angle shift and DC voltage are given as a function of active and reactive powers references according to (5), and they depend on the inductance's value and the grid voltage magnitude. Three operation modes can be obtained which are presented in Figure 9.

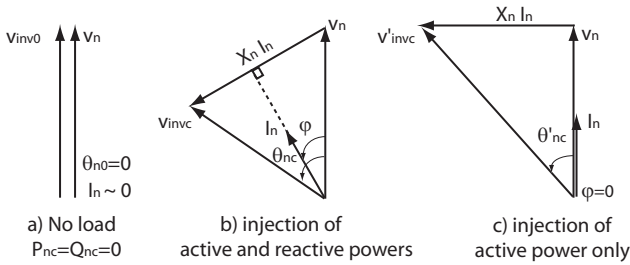


Figure 9. Diagram of voltage and current.

Starting from the active and reactive powers references, the system runs initially in no load operation, with active and reactive powers equal to zero (Figure 10). Both inverter and network voltages have the same phase where the amplitude is equal to nominal (Equation 6). Therefore the line current is very small (Figure 9-a).

$$\begin{cases} \theta_{n0} = 0 \\ V_{inv0} = V_n \Rightarrow U_{d0} = \frac{\pi}{2 \cos \delta_n} V_n \end{cases} \quad (6)$$

In the first transition at  $t = 0.4$  s, the network active and reactive powers are ramped to  $P_{ref} = S_n \times \cos \varphi$  and to  $Q_{ref} = S_n \times \sin \varphi$  respectively. Consequently, the angle shift and the DC voltage change from  $(\theta_{n0}, U_{d0})$  to  $(\theta_{nc}, U_{dc})$  (Figure 9-b and Figure 10). Their values depend on the active and reactive powers references (Equation 5).

In the second transition, at  $t = 10$  s, the reactive power ramps down to zero, as shown in Figure 10. Consequently, the angle shift and the DC voltage must change from  $(\theta_{nc},$

$U_{dc})$  to  $(\theta'_{nc}, U'_{dc})$ . Then the reactive power can be compensated and the system can be operated using a unity power factor.

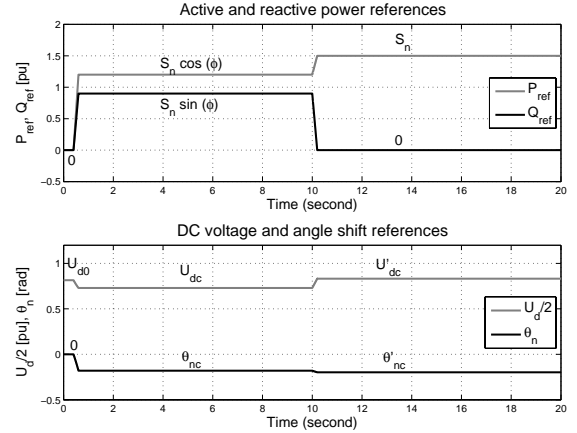


Figure 10. Network side references.

The system depicted in Figure 2 has been simulated using the following characteristics:  $V_n = 1pu$  is the network voltage.  $x_n = 0.2pu$ : inductance between inverter and network.  $\delta_n = 15.58^\circ$ : switching angle.  $S_n = 1.5pu$  is the apparent power. Figure 11 shows the simulated active and reactive powers for three operation modes. The line current is superposed on the network voltage when the reactive power is zero.

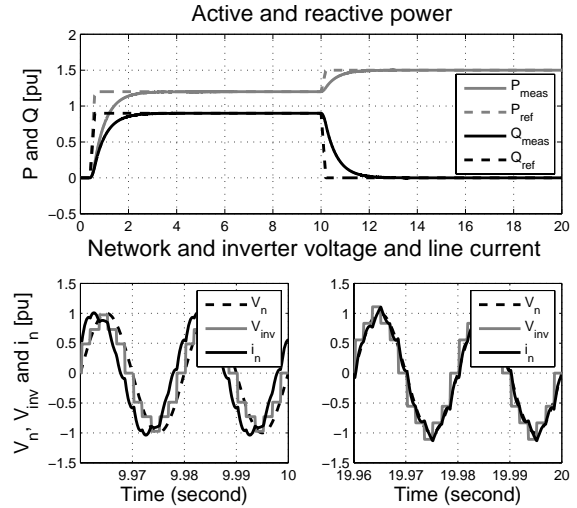


Figure 11. Simulation results.

### 4.2 Limitation and error control

It is important to notice in Figure 2 that the grid is represented by an ideal source with a fixed magnitude  $V_n$ . As a consequence, the open loop control strategy described on paragraph 4.1 gives good results. However, it is interesting to analyse what happens with a real system. For this reason,

the circuit shown in Figure 12 has been simulated under the same control strategy and using the same characteristics as in paragraph 4.1.

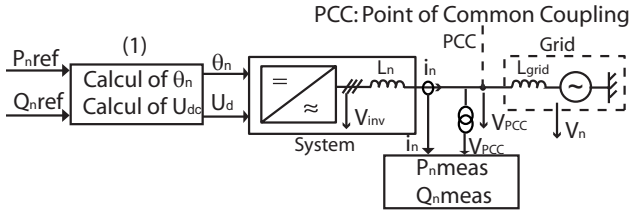


Figure 12. Open loop control circuit.

In comparison with Figure 2, the grid in Figure 12 contains an additional inductance  $L_{grid}$ . In this Figure,  $P_{meas}$  et  $Q_{meas}$  represent respectively active and reactive powers calculated according to (7) as a function of voltages and line currents measured at the PCC: (Point of Common Coupling).

$$\begin{cases} P_{meas} = V_{PCC1}i_{n1} + V_{PCC2}i_{n2} + V_{PCC3}i_{n3} \\ Q_{meas} = \frac{1}{\sqrt{3}}[(V_{PCC2}i_{n3} - V_{PCC3}i_{n2}) \\ + (V_{PCC3}i_{n1} - V_{PCC1}i_{n3}) \\ + (V_{PCC1}i_{n2} - V_{PCC2}i_{n1})] \end{cases} \quad (7)$$

Figure 13 shows the simulated active and reactive powers ( $P_{meas}$ ,  $Q_{meas}$ ) and their reference values ( $P_{ref}$ ,  $Q_{ref}$ ) for three operation modes. When changing the reference values, the measured active and reactive powers don't follow their references and they present a considerable error between measured and reference value.

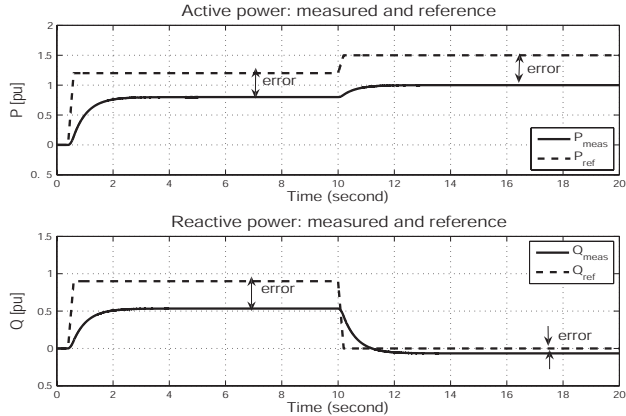


Figure 13. Open loop simulation result.

A simple method to avoid this error is to take the grid inductance value ( $X_{grid}$ ) into account when calculating the system references, i.e. angle shift and DC voltage. However, measuring the grid characteristic is not always possible. Then using an open loop control presents some control errors and limitations. This fact shows the importance of using a closed loop control strategy.

## 5. Closed loop control strategy

In order to avoid the deviation problem incurred by using an open loop control, a new control strategy is proposed in this section. The aim of the algorithm is to keep the powers close to their reference values, in other words, to minimize their errors. To achieve this goal, the produced active and reactive powers are controlled by using the closed loop circuit depicted in Figure 14.

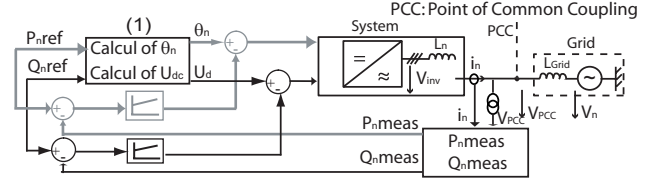


Figure 14. Closed loop control circuit.

The active power is controlled by acting on the angle shift between the grid and inverter output voltage, and the reactive power is controlled by adapting the DC voltage at the input of the inverter. By using a simple corrector, the error between the measured and reference signals can be compensated.

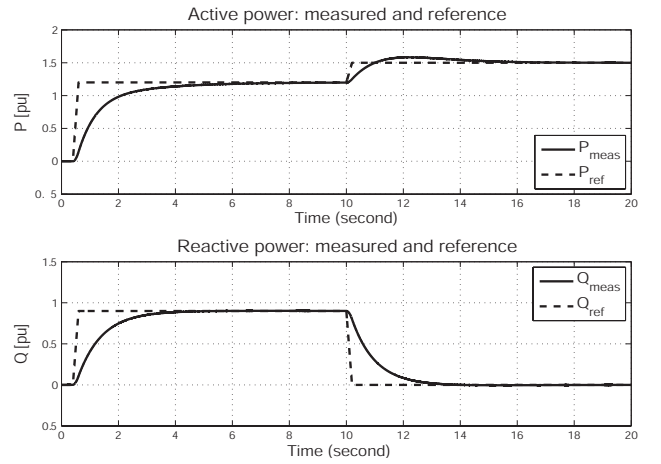


Figure 15. Closed loop simulation result.

Figure 15 shows the result: the active and reactive powers follow their references correctly, rapidly and nearly without any over shoot. This fulfilling result is visualized for the first and the second transition.

## 6. Partial experimental results

In order to validate the obtained result, a low-voltage laboratory prototype of the system depicted in Figure 2 has been built and tested (see Figure 16).

Figures 17 and 18 show the active and reactive powers measured respectively when  $\cos \varphi \neq 0$  and when  $\cos \varphi =$

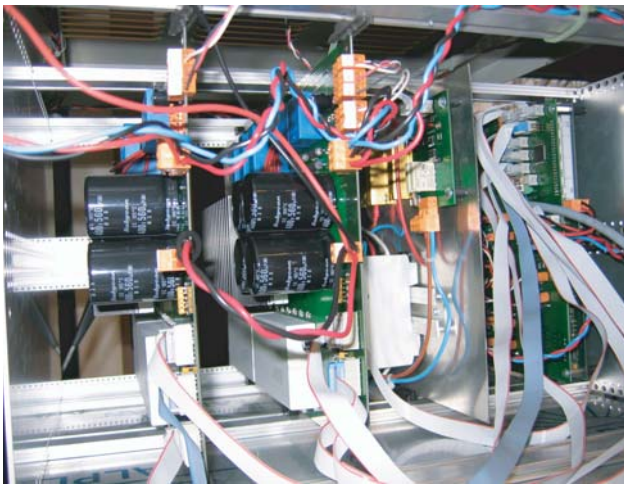


Figure 16. Laboratory prototype.

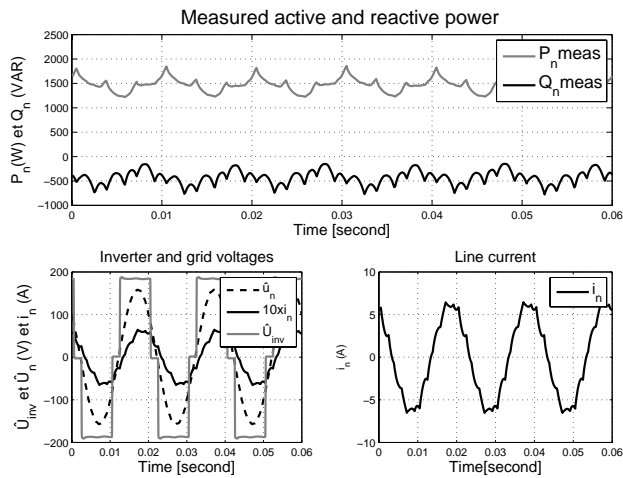


Figure 17. Measured active and reactive powers ( $Q_{nc} \neq 0$ ).

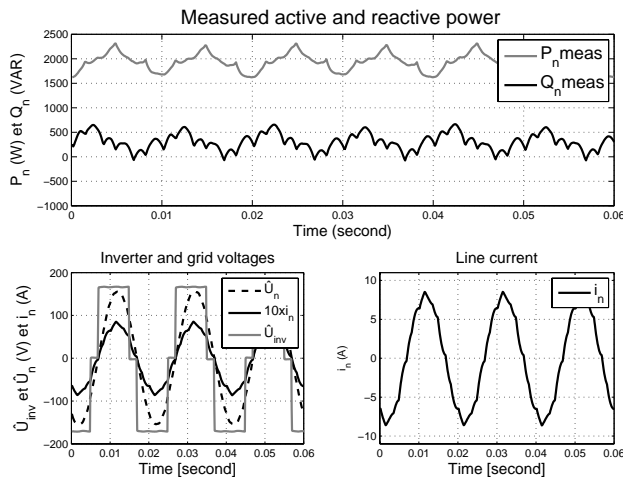


Figure 18. Measured active and reactive powers ( $Q_{nc} \approx 0$ ).

0. The line current is superposed on the network voltage, when the reactive power is near zero (see Figure 18).

## 7. Conclusion

In this paper, a new control strategy for a three level NPC inverter has been presented. It can be used for high power application and is characterized by a high efficiency. This efficiency is achieved by using a square wave modulation, which has the advantage of a quasi absence of switching losses. In this mode, only the frequency can be varied between the input and the output voltage, but their magnitudes are not freely controllable. The produced active and reactive powers can be controlled using a closed-loop control strategy: Active power is controlled by acting on the angle shift between the grid and output inverter voltages, and reactive power control is done by adapting the DC voltage at the input of the inverter. The contributions of this paper include a description of the control strategy using an open loop control circuit, a discussion of the properties and the limitation of the proposed method, as well as the corresponding characteristic curves obtained by using a closed-loop control strategy. Simulation and partial experimental results for different operating points and transitions between them highlight the capabilities of the proposed control strategy. These include the ability to operate high power application with unity power factor.

## References

- [1] R. Baker, "Bridge converter circuit," *United States Patent N. 4 270 163*, May 1981.
- [2] A. Nabae, I. Takahashi, and H. Akagi, "A new neutral-point-clamped PWM inverter," *IEEE Transactions on Industry Applications*, vol. IA - 17, pp. 518 – 523, September/October 1981.
- [3] A. Rufer and M. Veenstra, "Adapting alternating current or voltage produced by generator to network involves using frequency converter between generator and network, arrangement for regulating simulation field and phase angle," *Patent, DE 103 30 473 A1, Alstom Ltd, Switzerland, 2005*.
- [4] A. Benaboud, *Convertisseur de fréquence indirect à rapport de tension Pxe: interface entre turbo alternateurs à haute vitesse et réseau électrique*. thèse ep, no.3733, 2007: [http://biblion.epfl.ch/EPFL/theses/2006/3733/EPFL\\_TH3733.pdf](http://biblion.epfl.ch/EPFL/theses/2006/3733/EPFL_TH3733.pdf)
- [5] "ABB StakPak, H Series Press-pack IGBT 5SNR 20H2500," *ABB Industry: brochure and datasheet, Switzerland Ltd, 02 May 2004*.
- [6] H. Bühler, *Convertisseurs Statiques*. Lausanne: Presses Polytechniques et Universitaires Romandes, 1991.
- [7] A. Benaboud and A. Rufer, "New control strategy for three level npc converter connected to the grid," *Proceeding of the sixth IASTED International Conference*, pp. 400–405, 26-28 June 2006 Rhodes, Greece.